Coupled complex Ginzburg-Landau equations for the weak electrolyte model of electroconvection

Martin Treiber[1] and Lorenz Kramer[2]
[1]*Universität Stuttgart, 2. Institut für Theoretische Physik, Pfaffenwaldring 57, D-70569 Stuttgart, Germany*
[2]*Universität Bayreuth, Theoretische Physik II, Universitätsstraße 30, D-95440 Bayreuth, Germany*
(Received 4 August 1997; revised manuscript received 26 February 1998)

The recently introduced weak electrolyte model (WEM) has successfully explained many linear properties of electroconvection in planarly aligned nematic liquid crystals such as the crossover from a stationary to a Hopf bifurcation in the parameter range observed experimentally. Here we present the first weakly nonlinear analysis of the WEM providing the coefficients of the complex Ginzburg-Landau equation. Whereas the Hopf bifurcation is always supercritical, the stationary bifurcation is for typical materials subcritical, which appears to be in agreement with experiments. In the oblique-roll range the (complex) cross coupling coefficient between the two degenerate roll systems (''zig'' and ''zag'') are also calculated leading to the superposition of traveling rectangles as observed in recent experiments on the material I52. [S1063-651X(98)10807-3]

PACS number(s): 61.30.−v, 47.20.−k, 47.65.+a

I. INTRODUCTION

The traditionally used model for the electrohydrodynamic convection instability (EC) in nematic liquid crystal (NLC) layers [1,2] involves equations for the velocity field, the director, and the electric potential (or charge density). The NLC is considered as an anisotropic Ohmic conductor without specifying the origin of the conductivity. Otherwise the standard hydrodynamic description [3–5] is employed. This model, in particular in its three-dimensional formulation where rolls orienting obliquely to the planarly prealigned director (we here consider only this most common case) can be included [6–8], is referred to as the standard model (SM). For a general introduction, see, e.g., the books [5,9], or recent reviews [10].

The SM explains quantitatively the phenomena observed in the conduction range (low frequency of the applied ac voltage) if, roughly speaking, the cells are not too thin ($d \geqslant 50$ μm), or if one is not too near to threshold [7,8]. In contrast, some features observed in thinner cells near threshold remain unexplained even on a qualitative level. Most notable are traveling waves (TW), which have been observed as early as 1978 [11]. Later on, they were found by various groups in a broad parameter range in the NLCs MBBA [12,13], I52 [14,15], and in phase 5 [16,17]. TWs appear to be generic for relatively thin and clean cells and seem to be often favored by higher external frequencies (in particular near the cutoff frequency giving the crossover to the dielectric range). The SM, however, predicts always a stationary bifurcation.

Recently, the occurrence of the traveling waves and their linear properties have been explained by the weak electrolyte model (WEM) [18]. Specifically, a Hopf bifurcation to traveling waves was predicted for the above conditions, provided the recombination rate of mobile ions (see below) is sufficiently low. The Hopf frequency agreed quantitatively with experiments on the NLC's I52 [14], and phase 5 [19]. Also the behavior of MBBA appears to be well described [20].

Other unexplained features connect to nonlinear properties. Firstly, it is the slightly discontinuous (hysteretic) nature of the bifurcation that has been noted for some years under conditions where one is near the crossover between stationary and traveling waves [21,13,15,22–24] and which is in conflict with results for the SM [7,8]. Secondly, under conditions where the traveling rolls are manisfestly oblique, one has observed an extended form of spatiotemporal chaos (STC) [21,23,24], which in the material I52 clearly arises via a supercritical bifurcation. This system thus represents an example of ''STC at onset,'' which should be amenable to a quantitative analysis. Finally, under similar (but not the same) conditions, one can observe in I52 convection to arise in the form of wormlike localized structures [22,24].

In this work, we present the first results of the weakly nonlinear analysis of the WEM. Together with linear properties one can then derive the coefficients for the appropriate set of coupled complex Ginzburg-Landau equations (CCGL). In the experiments the interplay of the two variants of oblique rolls (''zig'' and ''zag'') appears to be more important than that of counterpropagating waves, which mostly suppress each other (see below). Therefore we have at this point calculated the saturation coefficient as well as the cross-coupling coefficient beween zig and zag, but not between counterpropagating waves. To our knowledge, this is the first system where the STC of the complex Ginzburg-Landau equations can be quantitatively compared with the experiment.

In Sec. II we sum up the WEM, in Sec. III the CCGL is derived, and comparison with experiments on I52 is done in Sec. IV. In Sec. V we give some conclusions and outlook. In Appendix A we summarize the director and velocity equations used both in the SM and the WEM. We also give analytic expressions for the threshold of the SM (Appendix B) and for the Hopf frequency (Sec. III with Appendix C). In Appendix D we present a set of effective equations that could be used as a starting point to go beyond the weakly nonlinear analysis in the WEM variables. Finally, in Appendix E we briefly make a connection with a generalized Swift-Hohenberg model introduced by Tu to describe the worm state [25].

II. THE WEAK-ELECTROLYTE MODEL

The equations of the WEM for the director and velocity fields are those of the SM, but the conduction properties are

explicitly modeled by introducing two species of oppositely charged ionic charge carriers. Without loss of generality we assume charges $\pm e$. The dynamics of the number densities $n^+(\boldsymbol{r},t)$ and $n^-(\boldsymbol{r},t)$ of the charge carriers is governed by drift relative to the fluid under an electric field and by a conventional dissociation-recombination reaction between neutral molecules and the ions. The mobility tensors $\underline{\underline{\mu}}^+$ and $\underline{\underline{\mu}}^-$ express the drift velocities in terms of the electric field, $\boldsymbol{v}^{\pm}_{\rm drift}=\pm\underline{\underline{\mu}}^{\pm}\boldsymbol{E}$. The tensors have the usual uniaxial-anisotropic form $\mu^{\pm}_{ij}\equiv\mu^{\pm}_{\perp}\mu'_{ij}=\mu^{\pm}_{\perp}(\delta_{ij}+n_in_j\sigma'_a)$, where n_i and n_j are components of the director, $\sigma'_a=\sigma^{\rm eq}_a/\sigma^{\rm eq}_{\perp}$ is the relative conduction anisotropy, and δ_{ij} is the Kronecker symbol. For simplicity the anisotropy of $\underline{\underline{\mu}}^+$ and $\underline{\underline{\mu}}^-$ are taken to be the same.

It is convenient to change from the fields $n^+(\boldsymbol{r},t)$ and $n^-(\boldsymbol{r},t)$ to the total space-charge density $\rho=e(n^+-n^-)$, which already appears in the SM, and the new field (''charge-carrier mode'') $\sigma_{\perp}(\boldsymbol{r},t)=e(\mu^+_{\perp}n^++\mu^-_{\perp}n^-)$ (we choose the one perpendicular to the director).

Neglecting diffusion and some small terms proportional to the difference $\mu^+_{\perp}-\mu^-_{\perp}$ of the mobilities, the balance equations for $\rho(\boldsymbol{r},t)$ and $\sigma_{\perp}(\boldsymbol{r},t)$ are [18]

$$\partial_t\rho+\boldsymbol{\nabla}\cdot(\boldsymbol{v}\rho+\underline{\underline{\mu}}'\boldsymbol{E}\sigma_{\perp})=0, \tag{1}$$

$$\partial_t\sigma_{\perp}+\boldsymbol{\nabla}\cdot(\boldsymbol{v}\sigma_{\perp}+\mu^+_{\perp}\mu^-_{\perp}\underline{\underline{\mu}}'\boldsymbol{E}\rho)=-\tau^{-1}_{\rm rec}(\sigma_{\perp}-\sigma^{\rm eq}_{\perp}). \tag{2}$$

The WEM equations consist of the Eqs. (1) and (2) supplemented by the equations of the SM for the director and velocity fields (Appendix A) together with the static conditions $\rho=\partial_i\epsilon_{ij}E_j$ with $\epsilon_{ij}=\epsilon_{\perp}\delta_{ij}+\epsilon_an_in_j$ (Poisson equation), $\boldsymbol{E}=\boldsymbol{E}_0(t)-\boldsymbol{\nabla}\phi$ (exploiting $\boldsymbol{\nabla}\times\boldsymbol{E}=\boldsymbol{0}$ and separating $\boldsymbol{E}$ into an external field and a distortion field), $\boldsymbol{n}^2=1$, and $\boldsymbol{\nabla}\cdot\boldsymbol{v}=\boldsymbol{0}$ (incompressibility). We will consider the common planar alignment and chose a coordinate system such that $\boldsymbol{n}=(1,0,0)$ at the upper and lower plates confining the NLC layer at $z=\pm d/2$. The external electric field from the applied ac voltage is then given by $\boldsymbol{E}_0(t)=[(\overline{V}\sqrt{2}/d)\cos\omega_0t]\boldsymbol{e}_z$ where $\overline{V}:=\sqrt{\overline{(V^2)}}$ is the effective voltage.

The six fields of the WEM are the potential ϕ of the electric field distortion (alternatively one can stay with ρ), the local conductivity $\sigma_{\perp}$, two director components (n_y and n_z), and two velocity fields or a suitable representation for them; see Eq. (18) below.

The WEM has four relevant time scales. The director-relaxation time $\tau_d=\gamma_1d^2/(K_{11}\pi^2)$ and the charge-relaxation time $\tau_q=\epsilon_0\epsilon_{\perp}/\sigma^{\rm eq}_{\perp}$ appear already in the SM. Here, γ_1 is a rotational viscosity, and K_{11} is the orientational elasticity for splay distortions. Typically, τ_d is $O(1\ {\rm s})$, and τ_q is $O(10^{-2}\ {\rm s})$. The WEM has two additional time scales [14,18]: a recombination time $\tau_{\rm rec}$ for the relaxation towards the equilibrium of the dissociation-recombination reaction where $\sigma_{\perp}(\boldsymbol{r},t)=\sigma^{\rm eq}_{\perp}$, and the transition time $\tau_t=d^2/(V_{c0}\mu^{\star})$ for a charge with the mobility $\mu^{\star}=\sqrt{\mu^+_{\perp}\mu^-_{\perp}}$ to traverse the cell under the applied voltage $V_{c0}=\sqrt{K_{11}/(\epsilon_0\epsilon_{\perp})}$, which is of the order of the critical voltage. The magnitude of τ_t is $O(0.1\ {\rm s})$. The interesting effects arise when $\tau_{\rm rec}$ is sufficiently large, typically $\approx O(10\ {\rm s})$.

Five dimensionless parameters characterize the dynamics: the control parameter $R=\overline{V}^2/V^2_{c0}$ or, alternatively, the distance from threshold $\epsilon=\overline{V}^2/\overline{V}^2_c-1$, the external frequency $\omega_0\tau_q$ in units of the inverse charge relaxation time, the ratio of the SM times τ_q/τ_d, the mobility parameter $\tilde{\alpha}=\pi\sqrt{\tau_q\tau_d/\tau^2_t}$, and the recombination parameter $\tilde{r}=\tau_d/\tau_{\rm rec}$. For small recombination rates, the Hopf frequency (21) predicted by the WEM is proportional to $\tilde{\alpha}/\tau_d=\pi\sqrt{\tau_q/(\tau_d\tau^2_t)}$.

III. COUPLED COMPLEX GINZBURG-LANDAU EQUATIONS

In this section, we scale lengths by d/π, and time by τ_d, if not explicitly stated otherwise. Furthermore, voltages are scaled by V_{c0}, conductivities by $\sigma^{\rm eq}_{\perp}$, dielectric permittivities by $\epsilon_0\epsilon_{\perp}$, the elastic constants K_{11}, K_{22}, K_{33} for splay, twist, and bend deformations by K_{11}, and the viscosities $\alpha_1,\ldots,\alpha_6$ (see Appendix A) by γ_1. We allow also for a magnetic field $\boldsymbol{H}$ and scale it to the splay Freédericksz transition field $H_F=\sqrt{K_{11}/(\chi_a\mu_0)}\,\pi/d$.

The linear analysis of the SM shows [7] that the patterns at threshold are either stationary normal rolls with wave vector $\boldsymbol{q}_c=(q_c,0)$, or a pair of stationary symmetry-degenerated oblique rolls with wave vectors $\boldsymbol{q}^{\rm zig}_c=(q_c,p_c)$ and $\boldsymbol{q}^{\rm zag}_c=(q_c,-p_c)$. The linear analysis of the WEM presented in the next subsection shows that these stationary modes can split into symmetry-degenerated pairs of left- and right-traveling rolls *via* a Hopf bifurcation. The kind of pattern depends on the NLC, the cell thickness, and the frequency of the applied voltage. Here, we consider the dynamics of right-traveling zig and zag oblique rolls. A reduction to the case of normal rolls is straightforward.

Near threshold ($\epsilon\ll1$), only modes with wave vectors near the critical ones are dynamically active. At lowest order, the amplitude expansion of the director n_z can be written as

$$n_z(\boldsymbol{r},t)=\tfrac{1}{2}[A(\boldsymbol{x},t)e^{ip_cy}+B(\boldsymbol{x},t)e^{-ip_cy}]e^{i(q_cx-\omega_Ht)}\cos z+{\rm c.c.} \tag{3}$$

To obtain the other fields one has to replace $\frac{1}{2}\cos z$ by the appropriate components of the linear eigenvector; see Eq. (20) below. The complex amplitudes A and B vary slowly in $\boldsymbol{x}=(x,y)$ and in t. They are defined so that their modulus gives the maximum director component n_z of the wave packets of the zig or zag modes, respectively. The component n_z can be measured with the help of the shadowgraph method [26].

For small $|A|$ and $|B|$ the dynamics of the amplitudes is governed by the coupled complex Ginzburg-Landau equations (CCGL)

$$\begin{aligned}\tau_0\partial_tA(\boldsymbol{x},t)&=\mathcal{L}(\boldsymbol{q}^{\rm zig}_c,\boldsymbol{\nabla}_x,\epsilon)A-g[(1+ic)|A|^2\\&\quad+h(1+ic_h)|B|^2]A,\\ \tau_0\partial_tB(\boldsymbol{x},t)&=\mathcal{L}(\boldsymbol{q}^{\rm zag}_c,\boldsymbol{\nabla}_x,\epsilon)B-g[(1+ic)|B|^2\\&\quad+h(1+ic_h)|A|^2]B.\end{aligned} \tag{4}$$

Here, g is the saturation coefficient, gc is the nonlinear frequency shift, and $h(1+ic_h)$ denotes the nonlinear coupling between the zig and zag waves.

The linear operator $\mathcal{L}(\boldsymbol{q}_c,\boldsymbol{\nabla}_x,\epsilon)=\tau_0[\lambda(\boldsymbol{q}_c-i\boldsymbol{\nabla}_x,\epsilon)-i\omega_H]$ is given in terms of the linear growth rate $\lambda(\boldsymbol{q},\epsilon)$ for the mode with wave vector $\boldsymbol{q}=(q,p)$ connected with the critical branch. In the range $|\boldsymbol{q}-\boldsymbol{q}_c^{\rm zig}|=O(\epsilon^{1/2})$, $|\boldsymbol{q}-\boldsymbol{q}_c^{\rm zag}|=O(\epsilon^{1/2})$, the Taylor expansion of $\mathcal{L}$ around $\epsilon=0$, $\boldsymbol{q}_c^{\rm zig/zag}=(q_c,\pm p_c)$ is given, up to $O(\epsilon)$, by

$$\begin{aligned}\mathcal{L}(\boldsymbol{q}_c^{\rm zig/zag},\boldsymbol{\nabla}_x,\epsilon)=&(1+i\tau_0\omega_\epsilon)\epsilon-\tau_0(v_{gx}\partial_x\pm v_{gy}\partial_y)\\&+\xi_{xx}^2(1+ib_{xx})\partial_x^2+\xi_{yy}^2(1+ib_{yy})\partial_y^2\\&\pm 2\xi_{xy}^2(1+ib_{xy})\partial_x\partial_y,\end{aligned}\tag{5}$$

with $\tau_0^{-1}=\partial{\rm Re}\lambda/\partial\epsilon|_c$, $\omega_\epsilon=\partial{\rm Im}\lambda/\partial\epsilon|_c$, $v_{gx}=\partial{\rm Im}\lambda/\partial q|_c$, $\xi_{xx}(1+ib_{xx})=-(\tau_0/2)\partial^2\lambda/\partial q^2|_c$, and $\xi_{xy}(1+ib_{xy})=-(\tau_0/2)\partial^2\lambda/(\partial q\partial p)|_c$. Here, $|_c$ means ''at threshold,'' $\boldsymbol{q}=\boldsymbol{q}_c^{\rm zig},\epsilon=0$. The expressions for $v_{gy},\xi_{yy}^2(1+ib_{yy})$, and $\xi_{xy}^2(1+ib_{xy})$ are analogous.

Let us summarize the scenario for the (primary) bifurcation of plane waves $A=A_0\exp i(-\Omega t+Qx+Py)$, $B=B_0\exp i(-\Omega t+Qx-Py)$ from the basic state [trivial solution of Eqs. (4)] as ϵ becomes positive; see e.g., [27]. For $Q=P=0$ one has either $|A_0|=\sqrt{\epsilon/g}$, $|B_0|=0$ (or vice versa), $\Omega=-\omega_\epsilon\epsilon+gc|A_0|^2/\tau_0$, i.e., zig or zag traveling rolls, or a symmetric superposition $|A_0|=|B_0|=\sqrt{\epsilon/[g(1+h)]}$, $\Omega=-\omega_\epsilon\epsilon+g(c+hc_h)|A_0|^2/\tau_0$ leading to traveling rectangles. These solutions bifurcate at $\epsilon=0$ and exist stably (relative to the trivial solution) for $\epsilon>0$ if the bifurcation is supercritical, i.e., for $g>0$ and $1+h>0$. For $h>1$ rolls are stable (relative to the rectangles), otherwise the rectangles are stable. For $(Q,P)\neq 0$ the bifurcation point is shifted upward to $\sigma=\epsilon-\xi_{xx}^2Q^2-\xi_{yy}^2P^2-2\xi_{xy}^2QP=0$ and the frequency is also shifted via the group velocity terms proportional to v_{gx} and v_{gy}, and the linear dispersion terms in Eq. (5).

A. Threshold and linear coefficients

It can be shown [20] that the nonconvecting basic state of the WEM (subscript 0) is given, in a good approximation, by $\phi_0=0$ (no induced electric potential), $\sigma_{\perp 0}=\sigma_\perp^{\rm eq}$ (the local conductivity equals the equilibrium conductivity), $\boldsymbol{n}_0=(1,0,0)$ (no director distortion), and $\boldsymbol{v}_0=0$ (no convection).

We obtain the threshold voltage, the Hopf frequency, and the linear coefficients of the amplitude equation (4) by linearizing the WEM equations around this basic state with the ansatz

$$\begin{aligned}\boldsymbol{E}&=[\pi^{-1}\sqrt{2R}\cos\omega_0 t]\boldsymbol{e}_z-\boldsymbol{\nabla}\phi_1(\boldsymbol{r},t):=\boldsymbol{E}_0(t)-\boldsymbol{\nabla}\phi_1(\boldsymbol{r},t),\\ \sigma_\perp&=\sigma_\perp^{\rm eq}+\sigma_1(\boldsymbol{r},t),\\ \boldsymbol{n}&=(1,0,0)+(0,n_{y1},n_{z1}),\quad \boldsymbol{v}=\boldsymbol{v}_1.\end{aligned}\tag{6}$$

Inserting this into the scaled WEM equations (1) and (2), into the z and y components of the director equation (A1), and into the z and y components of the curl of the equation for the velocity field (A2) gives the following linear system for the perturbations (subscript 1),

$$\left[\frac{\tau_q}{\tau_d}\partial_t\hat{\epsilon}+\hat{\sigma}\right]\phi_1+E_0\partial_z\sigma_1+\left[\frac{\tau_q}{\tau_d}\epsilon_a(\dot{E}_0+E_0\partial_t)+\sigma_aE_0\right]\partial_xn_{z1}=0,\tag{7}$$

$$[\tilde{\alpha}^2\pi^2E_0\partial_z]\hat{\epsilon}\phi_1+[\partial_t+\tilde{r}]\sigma_1+[\epsilon_a\tilde{\alpha}^2\pi^2E_0^2\partial_z]\partial_xn_{z1}=0,\tag{8}$$

$$\epsilon_a\pi^2E_0\partial_x\phi_1+[\partial_t+\hat{K}_{zz}-\epsilon_a\pi^2E_0^2]n_{z1}-(1-K_{22})\partial_z\partial_yn_{y1}+\alpha_3\partial_zv_{x1}+\alpha_2\partial_xv_{z1}=0,\tag{9}$$

$$-(1-K_{22})\partial_z\partial_yn_{z1}+[\partial_t+\hat{K}_{yy}]n_y+\alpha_3\partial_yv_{x1}+\alpha_2\partial_xv_{y1}=0,\tag{10}$$

$$\begin{aligned}&-\alpha_3\partial_y\partial_z\partial_tn_{z1}+[\alpha_2\partial_x^2-\alpha_3\partial_y^2]\partial_tn_{y1}\\&\quad-[(\alpha_1+\alpha_6+\eta_1)\partial_x^2+\eta_2(\partial_y^2+\partial_z^2)]\partial_yv_{x1}\\&\quad+\left[\eta_1\partial_x^2-(\eta_2-\alpha_3-\alpha_4)\partial_y^2+\frac{\alpha_4}{2}\partial_z^2\right]\partial_xv_{y1}\\&\quad+\left[\frac{\alpha_3-\alpha_6}{2}\right]\partial_x\partial_y\partial_zv_{z1}=0,\end{aligned}\tag{11}$$

$$\begin{aligned}&\pi^2E_0\partial_x\hat{\epsilon}\phi_1+[(\alpha_2\partial_x^2-\alpha_3\partial_z^2)\partial_t+\epsilon_a\pi^2E_0^2\partial_x^2]n_{z1}\\&\quad-\alpha_3\partial_y\partial_z\partial_tn_{y1}-[(\alpha_1+\alpha_6+\eta_1)\partial_x^2+\eta_2(\partial_y^2+\partial_z^2)]\partial_zv_{x1}\\&\quad+\left[\frac{\alpha_3-\alpha_6}{2}\right]\partial_x\partial_y\partial_zv_{y1}\\&\quad+\left[\eta_1\partial_x^2+\frac{\alpha_4}{2}\partial_y^2+(\alpha_3+\alpha_4-\eta_2)\partial_z^2\right]\partial_xv_{z1}=0.\end{aligned}\tag{12}$$

Here, we used the abbreviations (note that $K_{11}=\sigma_\perp^{\rm eq}=\epsilon_0\epsilon_\perp=1$)

$$\begin{aligned}\hat{\epsilon}&=-[(1+\epsilon_a)\partial_x^2+\partial_y^2+\partial_z^2],\\ \hat{\sigma}&=-[(1+\sigma_a)\partial_x^2+\partial_y^2+\partial_z^2],\end{aligned}\tag{13}$$

$$\hat{K}_{zz}=-[K_{33}\partial_x^2+K_{22}\partial_y^2+\partial_z^2]+H_x^2-H_z^2,\tag{14}$$

$$\hat{K}_{yy}=-[K_{33}\partial_x^2+\partial_y^2+K_{22}\partial_z^2]+H_x^2-H_y^2,\tag{15}$$

and the Miesowicz coefficients

$$\eta_1=(-\alpha_2+\alpha_4+\alpha_5)/2,\quad \eta_2=(\alpha_3+\alpha_4+\alpha_6)/2.\tag{16}$$

Only one of the Cartesian components H_i of the scaled magnetic field is allowed to be nonzero. The BCs at $z=\pm\pi/2$ are

$$\phi_1=\partial_z\sigma_1=n_{z1}=n_{y1}=\boldsymbol{v}_1=0.\tag{17}$$

The incompressibility condition $\boldsymbol{\nabla}\cdot\boldsymbol{v}=0$ is satisfied by expressing the velocity by the toroidal and poloidal potentials G_t and G_p for divergence-free fluids [28],

$$\boldsymbol{v}_1=\boldsymbol{\nabla}\times(G_{t1}\boldsymbol{e}_z)+\boldsymbol{\nabla}\times[\boldsymbol{\nabla}\times(G_{p1}\boldsymbol{e}_z)].\tag{18}$$

The equations (7)–(12) with (18) represent a linear system with time-periodic coefficients for the fields $\phi_1, \sigma_1, n_{z1}, n_{y1}, G_{t1}$, and G_{p1}. It is converted to an algebraic eigenvalue system for the complex growth rate λ by using lowest-order Fourier modes in x, y, and t, and lowest-order Galerkin modes satisfying Eq. (17) in $z \in [-\pi/2, \pi/2]$,

$$(\phi_1, \sigma_1, n_{z1}, n_{y1}, G_{t1}, G_{p1})^T = \boldsymbol{w}^{\mathrm{zig}}(z,t) e^{i(qx+py)+\lambda t}, \quad (19)$$

$$\boldsymbol{w}^{\mathrm{zig}}(z,t) = \begin{pmatrix} (\phi^+ \cos\,\omega_0 t + \phi^- \sin\,\omega_0 t)\cos z \\ \sigma^{(0)} \sin z \\ n_z^{(0)} \cos z \\ n_y^{(0)} \sin 2z \\ G_t^{(0)} \sin 2z \\ G_p^{(0)} C_1(z) \end{pmatrix}, \quad (20)$$

where $C_1(z)$ is the first Chandrasekhar function [29].

For given material and system parameters and for a given external frequency ω_0, the complex growth rate depends on R, q, and p. The neutral surface $R_0(q,p)$ is defined by a vanishing real part of the growth rate, $\mathrm{Re}\lambda(R_0,q,p)=0$. The threshold R_c, and the associated critical wave numbers q_c and p_c are given by the minimum of the neutral surface with respect to q and p. Also the coherence lengths can be obtained from the relation

$$\xi_{xx}^2 = \frac{1}{2R_c}\frac{d^2R_0}{dq^2}, \quad \xi_{yy}^2 = \frac{1}{2R_c}\frac{d^2R_0}{dp^2}, \quad \xi_{xy}^2 = \frac{1}{2R_c}\frac{d^2R_0}{dqdp},$$

where the derivatives are to be taken at q_c, p_c.

For high recombination rates $\tilde{r}$, the WEM predicts a stationary bifurcation. In the limit $\tilde{r}\to\infty$, the SM is recovered. For this case, we derived an intuitively appealing analytic expression for the neutral surface, see Appendix B. For sufficiently low recombination rates, the WEM predicts a Hopf bifurcation, i.e., the growth rate at threshold ($\mathrm{Re}\lambda|_c = 0$) has a nonzero imaginary part $\omega_H = \mathrm{Im}\lambda|_c$, and only then are the coefficients of the CCGL (4) complex.

Figure 1 shows the threshold values $\overline{V}_c$, ω_H, q_c, and p_c for the NLC I52 as obtained by solving the algebraic eigenvalue system (7)–(12) with (19) and (20). Shown is the limit of low external frequency $\omega_0\tau_q \ll 1$ as a function of the inverse recombination time $\tilde{r}$, the only essential parameter of the WEM that is not known from independent measurements [19]. Besides a nonzero Hopf frequency for small values of $\tilde{r}$, the WEM predicts a small shift of the threshold with respect to the SM, and shifts of q_c and p_c.

We derived simple approximate analytic expressions for the Hopf frequency, the threshold shift, and the linear CCGL parameters as a function of $\tilde{r}$. These expressions are valid for $\tilde{\alpha} \ll 1$, which is usually fulfilled, and not too near to the codimension-two point $\tilde{r}_{C2}$ separating the oscillatory from the stationary regime. For the parameters of Fig. 1, the error of these expressions is less than 2%. The analytic expression for the Hopf frequency is given by [compare Fig. 1(a)]

$$\omega_H = \sqrt{\tilde{\omega}^2 - \tilde{r}^2}, \quad \tilde{r} \leqslant \tilde{\omega}. \quad (21)$$

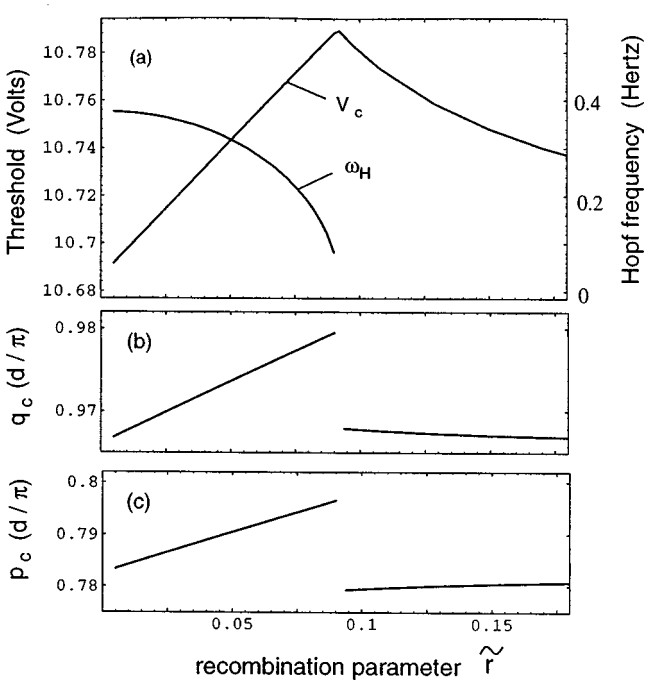

FIG. 1. Threshold diagram as predicted by the WEM for a cell of the nematic I52 ($d = 28\ \mu$m) at 60 °C as a function of the inverse recombination time $\tilde{r} = \tau_d/\tau_{\mathrm{rec}}$ for $\omega_0\tau_q \ll 1$. (a) Threshold voltage and (Hopf) frequency of the traveling rolls at threshold. (b) Component of the wave vector parallel to the director, and (c) perpendicular to the director. At the value $\tilde{r}_{C2} = 0.91$, there is a codimension-two point leading from the oscillatory regime ($\tilde{r} < \tilde{r}_{C2}$) to the stationary regime ($\tilde{r} > \tilde{r}_{C2}$).

In physical units, $\tilde{r} = 1/\tau^{\mathrm{rec}}$, and $\tilde{\omega} = \omega_H(\tilde{r}=0)$ is given by [19]

$$\tilde{\omega} = \pi C' \frac{\overline{V}_c^2 \epsilon_0 \epsilon_\perp}{d^3(1+\omega'^2)} \sqrt{\frac{\mu_\perp^+ \mu_\perp^-}{\gamma_1 \sigma_\perp^{\mathrm{eq}}}}. \quad (22)$$

Here, C' is a dimensionless factor of order unity given in Appendix C, and $\omega' = \omega_0\tau_q(1+\boldsymbol{q}_c^2 + \epsilon_a q_{cx}^2)/(1+\boldsymbol{q}_c^2 + \sigma_a q_{cx}^2)$.

The approximate expression for the threshold shift, Fig. 1(a), is

$$\Delta\epsilon \equiv \frac{\overline{V}_c^2}{(\overline{V}_c^{\mathrm{SM}})^2} - 1 = \begin{cases} \tau_0^{\mathrm{SM}} \tilde{r}, & \tilde{r} \leqslant \tilde{\omega} \\ \tau_0^{\mathrm{SM}} \tilde{\omega}^2/\tilde{r}, & \tilde{r} > \tilde{\omega}. \end{cases} \quad (23)$$

The correlation time τ_0 in the CCGL (4) is approximately given by [30]

$$\tau_0 = \begin{cases} 2\tau_0^{\mathrm{SM}}, & \tilde{r} \leqslant \tilde{\omega} \\ \tau_0^{\mathrm{SM}}\left(1 - \dfrac{\tilde{\omega}^2}{\tilde{r}^2}\right), & \tilde{r} > \tilde{\omega}. \end{cases} \quad (24)$$

The factor of 2 in the correlation time in the Hopf regime should be accessible to experiments. The correlation lengths ξ_{xx}, ξ_{xy}, and ξ_{yy} are the same as in the SM [30]. The group velocities and linear dispersions in the Hopf regime ($\tilde{r} < \tilde{\omega}$)

can be expressed in terms of the group velocities and the Hopf frequency $\tilde{\omega}$ for zero recombination [30],

$$v_{gi}=\frac{\tilde{\omega}}{\omega_H}v_{gi}(\tilde{r}=0), \quad b_{ij}=-\tilde{r}/\omega_H, \quad \tilde{r}<\tilde{\omega}, \qquad (25)$$

where i,j stand for x or y.

The general expression for τ_0^{SM} is too complicated to be given here. However, for normal rolls one has $\tau_0^{\mathrm{SM}}=-1/\lambda_{0z}$, where λ_{0z} is given in Appendix C. Actually this relation provides a good estimate of τ_0^{SM} also for $p_c\neq 0$ (the error is typically less than 10%).

B. Nonlinear coefficients

We calculate the nonlinear coefficients of Eq. (4) by a systematic amplitude expansion of the WEM equations. Denoting the fields ϕ, $\sigma_\perp$, n_z, n_y, G_t, and G_p by a formal vector $\boldsymbol{u}$, the WEM equations (1), (2), (A1), and (A2) can be written symbolically as

$$\underline{\underline{B}}\,\partial_t\boldsymbol{u}=\underline{\underline{L}}\,\boldsymbol{u}+\boldsymbol{N}_2(\boldsymbol{u},\boldsymbol{u})+\boldsymbol{N}_3(\boldsymbol{u},\boldsymbol{u},\boldsymbol{u})+\cdots. \qquad (26)$$

The linear matrix-differential operators $\underline{\underline{B}}$ and $\underline{\underline{L}}$ are defined explicitly by the Eqs. (7)–(12) with Eq. (18). The nonlinear operators $\boldsymbol{N}_2$ and $\boldsymbol{N}_3$ have, respectively, several hundred and some thousand terms, so the derivation of the nonlinear coefficients can be presented only schematically; for an effective model, see Appendix D. The fields are expanded in the amplitudes A and B, $\boldsymbol{u}=\boldsymbol{u}^{(1)}+\boldsymbol{u}^{(2)}+\cdots$ with

$$\boldsymbol{u}^{(1)}=A\boldsymbol{w}^{\mathrm{zig}}(z,t)e^{i(q_cx+p_cy-\omega_Ht)}+B\boldsymbol{w}^{\mathrm{zag}}(z,t)e^{i(q_cx-p_cy-\omega_Ht)}+\mathrm{c.c.} \qquad (27)$$

The functions $\boldsymbol{w}^{\mathrm{zig}}$ and $\boldsymbol{w}^{\mathrm{zag}}$ are the eigenfunctions of the Fourier-transformed linear WEM equations at $\boldsymbol{q}=(q_c,\pm p_c)$, normalized such that the n_z component of Eq. (27) is identical to Eq. (3). As in the linear calculations, we used Eq. (20) for $\boldsymbol{w}^{\mathrm{zig}}$ and a corresponding expansion for $\boldsymbol{w}^{\mathrm{zag}}$.

The further procedure is canonical [31]. At second order in the amplitudes one obtains for $\boldsymbol{u}^{(2)}$ the inhomogeneous equation $(\underline{\underline{B}}\,\partial_t-\underline{\underline{L}})\boldsymbol{u}^{(2)}=\boldsymbol{N}_2(\boldsymbol{u}^{(1)},\boldsymbol{u}^{(1)})$. To solve for $\boldsymbol{u}^{(2)}$, we used expansions analogous to Eq. (20), but with the opposite z symmetries. The dependence of $\boldsymbol{u}^{(2)}$ on $\boldsymbol{x}$ and t are given by $\exp[in(q_cx-\omega_Ht)+imp_cy]$ with $n,m=-2,0,2$. At third order in the amplitudes, the inhomogeneity of the equation for $\boldsymbol{u}^{(3)}$, given by $\boldsymbol{N}_2(\boldsymbol{u}^{(1)},\boldsymbol{u}^{(2)})+\boldsymbol{N}_2(\boldsymbol{u}^{(2)},\boldsymbol{u}^{(1)})+\boldsymbol{N}_3(\boldsymbol{u}^{(1)},\boldsymbol{u}^{(1)},\boldsymbol{u}^{(1)})$, has ''resonant'' terms proportional to $e^{i(q_cx\pm p_cy-\omega_Ht)}$ that lie in the kernel of the adjoint linear operator. The ensuing solvability conditions lead to the nonlinear parts of the CCGL (4).

In Figs. 2 and 3 the nonlinear coefficients are plotted as a function of the inverse recombination time $\tilde{r}$ (solid lines). There are three regions. In the oscillatory (Hopf) range $\tilde{r}<\tilde{r}_{C2}\approx\tilde{\omega}$, the nonlinear saturation coefficients g and $g(1+h)$ are positive, so that the bifurcation is always continuous, see the discussion after Eqs. (4) and (5). The cross coupling h is smaller than 1, so the WEM predicts that zig ($B=0$) or zag ($A=0$) traveling rolls are unstable with respect to a superposition where $A=B$. The nonlinear dispersion c is positive with the consequence that the frequency of the traveling waves decreases with the amplitude. In a range $\tilde{r}_{C2}<\tilde{r}_{\mathrm{tri}}$, the Hopf frequency is zero and both g and $g(1+h)$ are negative, so the bifurcation is predicted to be stationary hysteretic. At the tricritical point $\tilde{r}_{\mathrm{tri}}$, the saturation becomes positive and for $\tilde{r}>\tilde{r}_{\mathrm{tri}}$, one has a continuous stationary bifurcation. On increasing $\tilde{r}$ further, one approaches the SM [30].

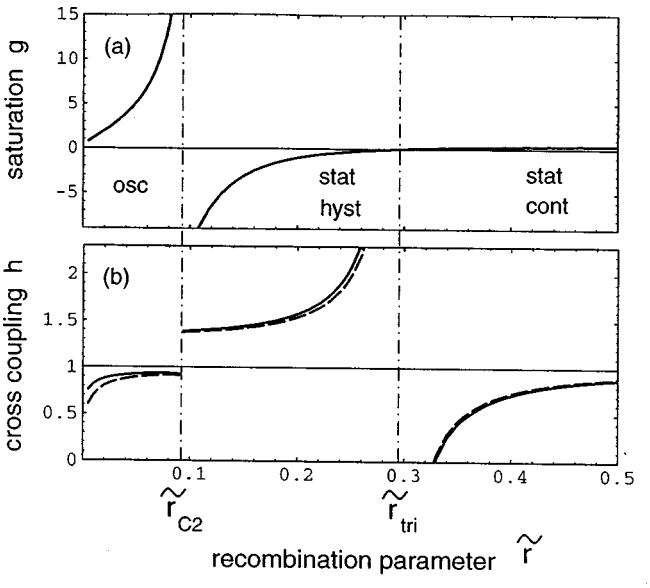

FIG. 2. Real parts of the nonlinear coefficients of the CCGL (4) as a function of $\tilde{r}=\tau_d/\tau_{\mathrm{rec}}$ for the material parameters of I52 at 60 °C. Shown are the results of the (lowest-order) nonlinear calculations with all nonlinearities of the WEM equations (full lines), and with the effective nonlinearities of Eq. (D2) (dashed). For the saturation coefficient g the difference is too small to be visible. The three regions, oscillatory, stationary hysteretic, and stationary continuous, are separated by the codimension-two point $\tilde{r}_{C2}$, and the tricritical point $\tilde{r}_{\mathrm{tri}}=0.295$ where the saturation coefficient g vanishes.

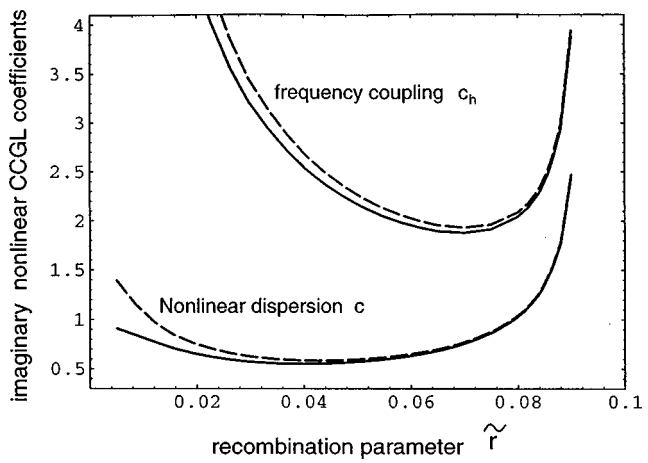

FIG. 3. Imaginary parts of the nonlinear coefficients of the CCGL (4) in the oscillatory regime, $\tilde{r}<\tilde{r}_{C2}$. The material parameters and the denotation of the lines are the same as in Fig. 2. The sign of the nonlinear dispersion c is defined such that for $c>0$ the frequency decreases with the amplitude.

IV. COMPARISON WITH EXPERIMENTS

In recent expriments on the NLC I52, three scenarios for the primary bifurcation were found, depending on the temperature and the cell thickness [14,22,23]. For low temperatures and relatively thin cells, the primary bifurcation was to a localized traveling-wave state called ''worms'' [22]. For higher temperatures (higher conductivities), the bifurcation was to a chaotic extended traveling-wave state. For even higher temperatures (conductivities) or for thick cells, the primary bifurcation was to a stationary state. The experiments were in the regime of oblique rolls. The worm state consisted of a superposition of either left- or right-traveling zig and zag rolls. The extended chaotic state often involves the same two modes, and the stationary state was a superposition of stationary zig and zag rolls. The oscillatory states bifurcated continuously (the worm state, at least, in a statistical sense), while the stationary state showed a hysteresis. On increasing ϵ, the frequency of the traveling rolls decreased [24], and between $\epsilon=0.03$ (high $\sigma_\perp^{\rm eq}$) and $\epsilon=0.1$ (low $\sigma_\perp^{\rm eq}$), there was a secondary bifurcation to a stationary state [22].

Most of these results can be explained, at least qualitatively, within the framework of the CCGL with coefficients derived from the WEM.

Figure 4 shows the WEM predictions for $d=28$ μm (most experiments were made on cells of this thickness), as a function of temperature, here replaced by the conductivity $\sigma_\perp^{\rm eq}$. For high values of $\sigma_\perp^{\rm eq}$, there is a transition to the stationary regime, in qualitative agreement with the experiments. The recombination parameter is chosen such that this transition occurs at the experimentally observed value $\sigma_\perp^{\rm eq}\approx 2\times 10^{-8}(\Omega\ {\rm m})^{-1}$. For simplicity we assume for the recombination rate $\tau_{\rm rec}^{-1}$ the same temperature dependence as for the viscosity γ_1, which leads to a constant recombination parameter $\tilde{r}=0.07$.

Figures 4(a) and 4(b) contain two predictions that agree qualitatively with the experiments:

(i) g and $g(1+h)$ are >0 in the Hopf regime (continuous bifurcation) and <0 in the stationary regime (hysteretic bifurcation).

(ii) In the Hopf regime the cross-coupling coefficient h is smaller than 1, so isolated zig and zag rolls are unstable with respect to a superposition to traveling rectangles, in agreement with the experiment. (the cross-coupling coefficient to the left-traveling waves is not yet calculated).

The nonlinear imaginary coefficients c and c_h are positive in the Hopf regime. They both increase when the conductivity approaches the value of the $C2$ point. They are decisive for the question of the modulational stability of the traveling rectangles in the oscillatory range. Whereas it is easy to see that the Newell criterion $b_{xx}c+1<0$ for the Benjamin-Feir instability of traveling waves (the rectangles travel in the x direction) is satisfied near the codimension-two point, the corresponding criterion for standing waves $b_{yy}(c-h^2c_h)+1-h^2<0$ is not [32,33].

Figure 5(a) shows, for the same system as in Fig. 4, the ''total frequency-shift factor''

$$\frac{d\omega}{d\epsilon}=\tau_d^{-1}\left(\omega_\epsilon-\frac{c}{\tau_0}\right) \tag{28}$$

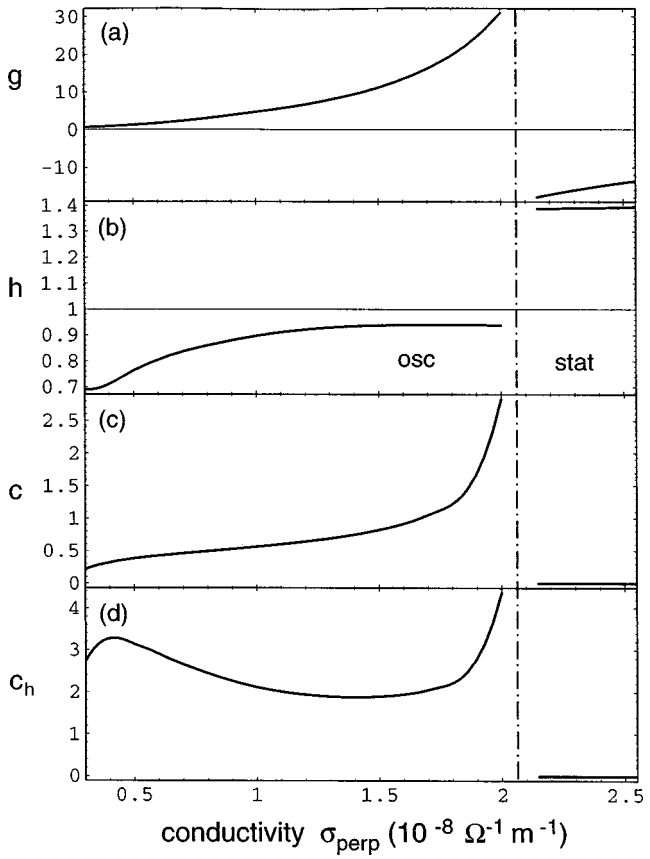

FIG. 4. Nonlinear coefficients as a function of the equilibrium conductivity $\sigma_\perp^{\rm eq}$ for I52 with $\tilde{r}=0.07$ and the other material parameters depending on $\sigma_\perp^{\rm eq}$ in accordance with the experiments in Ref. [22]. There, $\sigma_\perp^{\rm eq}$ is varied by varying the temperature. The parameters are taken at the corresponding temperature, e.g., 31 °C for $\sigma_\perp^{\rm eq}=0.3\times 10^{-8}(\Omega\ {\rm m})^{-1}$, and 62 °C for $\sigma_\perp^{\rm eq}=1.6\times 10^{-8}(\Omega\ {\rm m})^{-1}$. (a) Saturation coefficient g and (b) cross coupling h. For $h<1$ ($h>1$), a superposition of zig and zags (either zig or zag rolls) are expected. (c), (d) Imaginary parts of the nonlinear coefficients.

at $\epsilon=0$. The first term ω_ϵ results from the linear frequency shift $\partial{\rm Im}(\lambda)/\partial\epsilon$, and the second term from the nonlinear frequency shift $\partial\omega/\partial|A|^2\partial|A|^2/\partial\epsilon$. The predicted decrease for 41 °C [$\sigma_\perp^{\rm eq}=0.8\times 10^{-8}(\Omega\ {\rm m})^{-1}$] agrees nearly quantitatively with the measured decrease of $d\omega/d\epsilon=-10\ {\rm s}^{-1}$ [34].

Figure 5(b) shows the value $\epsilon_{\rm stat}$ where an extrapolation of the frequency decrease would lead to a zero frequency. The curve is comparable with the experimental bifurcation diagram in [22] for the secondary bifurcation to a stationary state.

Figure 6 shows a summary of the weakly nonlinear WEM predictions. The arrow from A to C shows the range of system parameters covered in the experiments [22], the arrow from A to B shows the change when the cell thickness is doubled.

V. CONCLUDING REMARKS

We have presented a weakly nonlinear analysis of the WEM model for electroconvection in NLC. One may conclude that this model, which has been the only one to describe the traveling rolls observed in the experiments, also

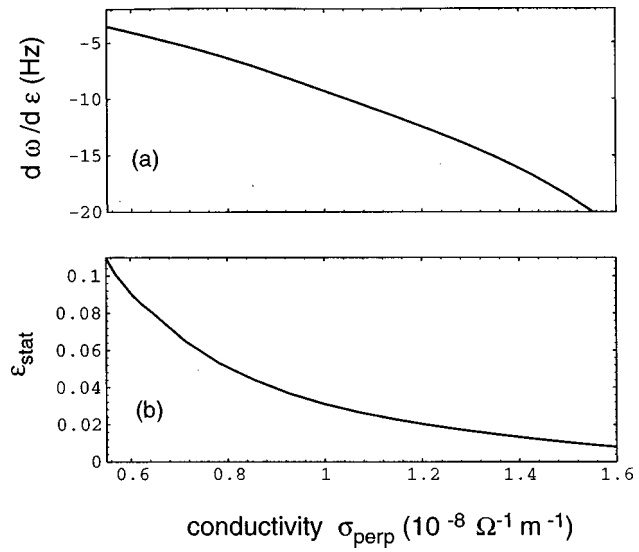

FIG. 5. Total frequency-shift factor $d\omega/d\epsilon$ at $\epsilon=0$ for the same material parameters as in Fig. 4. (b) Value of the control, parameter, where a linear extrapolation of the frequency decrease would lead to a vanishing frequency.

allows one to describe many of the weakly nonlinear properties observed in experiment. Hopefully also the remaining open problems can be resolved, e.g., the extended chaos [23,24], which are possibly described by the coupled complex Ginzburg-Landau equations (4). Then there is the worm state [22,24], where in spite of the forward bifurcation (Hopf range) higher-order terms are presumably needed.

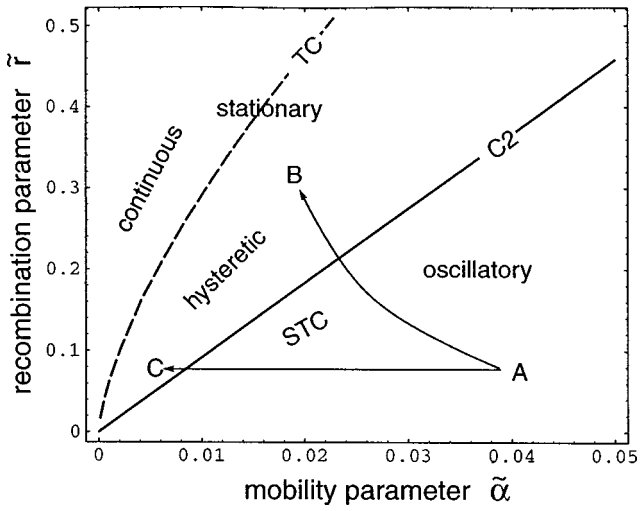

FIG. 6. Phase diagram as derived from the weakly nonlinear analysis in the $(\tilde{\alpha},\tilde{r})$ plane using parameters for I52 at 45 °C, and for external frequencies satisfying $\omega_0\tau_q \ll 1$. The curve labeled $C2$ is the codimension-two curve $\tilde{r}=\tilde{\omega}$ separating the Hopf regime of traveling waves from the stationary regime. On the stationary side, the bifurcation is hysteretic in a rather large region bounded by the $C2$ curve and the tricritical curve labeled TC. In the limit $\tilde{r}\to\infty$, the SM behavior is recovered. The point A corresponds to the experiments of Ref. [22] at 30 °C. The arrow to point C indicates the change in the space $(\tilde{\alpha},\tilde{r})$ on increasing the temperature to 60 °C assuming a constant recombination parameter. The arrow to point B corresponds to doubling the cell thickness.

The CCGL presented here is not applicable in the range where the bifurcation is subcritical, i.e., on the stationary side of the codimension-two ($C2$) point. However, also on the Hopf side (and very near to the $C2$ point) higher-order terms are important, because, roughly speaking, with increasing amplitude, the Hopf branch very quickly collides with the subcritical stationary branch, which persists across the $C2$ point. In fact, slightly above the $C2$ point one can have the situation where the Hopf branch is not accessible at all. This was apparently the case in experiments on MBBA where the Hopf bifurcation has been identified by observing the (thermal) fluctuations slightly below threshold [13].

To understand these and other phenomena occurring near the $C2$ point (like the worm state [22,24] or the hysteretic jump to stationary rolls after a short forward Hopf branch observed in phase 5 [21,35]) it is important to go beyond the lowest-order weakly nonlinear approximation where the slow charge carrier mode is treated adiabatically. By treating the charge carrier mode dynamically and coupling it to the Ginzburg-Landau equations one may be able to describe these phenomena. A possible starting point for such an analysis in the form of effective nonlinear WEM equations is presented in Appendix D. The situation is reminiscent of that in thermal convection of binary mixtures where it proved useful to separate out the slow concentration field [36]. Indeed here it was shown that stable localized solutions in 1D could exist even when the bifurcation is supercritical [37].

Recently, a generalized Swift-Hohenberg equation for a *subcritical* Hopf bifurcation has been proposed to model the worm state [25]. Solutions (mostly simulational) were presented that do show features similar to the worms. Although these solutions may indeed capture some of the observed features, the model is clearly at conflict with the theory as derived from the underlying hydrodynamics. Nevertheless we attempt to make some contact in Appendix E.

On a more basic level it would seem desirable to provide a more stringent test of the WEM by direct measurement of the most important unknown parameter, namely, the recombination time $\tau_{\rm rec}$ of the mobile ions, in situations where traveling rolls can arise. Here we have fitted $\tau_{\rm rec}$ to get agreement with the observed $C2$ point. The only measurements we are aware of in a relevant material (MBBA) were done above the clearing point, giving $\tau_{\rm rec}>10^4$ s [38].

ACKNOWLEDGMENTS

We wish to thank W. Pesch for useful discussions. Financial support from the DFG (Grant No. Kr690/12 and Graduiertenkolleg ''Nichtlineare Spektroskopie und Dynamik''), and the TMR network ''Patterns, Noise & Chaos,'' is gratefully acknowledged.

APPENDIX A: THE EQUATIONS FOR THE DIRECTOR AND THE FLUID VELOCITY

The dynamic equations for the director $\boldsymbol{n}(\boldsymbol{r},t)$ and the fluid velocity $\boldsymbol{v}(\boldsymbol{r},t)$ used both in the SM and in the WEM are the Erickson-Leslie equations

$$\gamma_1(\partial_t+\boldsymbol{v}\cdot\boldsymbol{\nabla}-\boldsymbol{\omega}\times)\boldsymbol{n}=-\underline{\underline{\delta}}^{\perp}[\boldsymbol{h}+(\alpha_2+\alpha_3)\underline{\underline{A}}\boldsymbol{n}, \quad \text{(A1)}$$

$$\rho_m(\partial_t+\boldsymbol{v}\cdot\boldsymbol{\nabla})v_i=-\partial_i p-\partial_j(\pi_{ij}+T_{ij}^{\rm visc})+\rho E_i. \quad \text{(A2)}$$

Equation (A1) describes the balance of the torques acting on the director. Hydrodynamic torques come from the local fluid rotation $\boldsymbol{\omega}=(\boldsymbol{\nabla}\times\boldsymbol{v})/2$ and from the hydrodynamic shear $A_{ij}=(\partial_i v_j+\partial_j v_i)/2$. The projection tensor $\delta_{ij}^{\perp}=\delta_{ij}-n_i n_j$ guarantees $n^2=1$. The rotational viscosity $\gamma_1=\alpha_3-\alpha_2$ is a combination of the Leslie coefficients $\alpha_1\cdots\alpha_6$ to be introduced below. The reversible torques are described by the ''molecular field''

$$h_i=\frac{\partial F}{\partial n_i}-\frac{\partial}{\partial x_j}\left(\frac{\partial F}{\partial n_i/\partial x_j}\right). \quad \text{(A3)}$$

where the density of the free enthalpy

$$F=\frac{1}{2}\{K_{11}(\boldsymbol{\nabla}\cdot\boldsymbol{n})^2+K_{22}[\boldsymbol{n}\times(\boldsymbol{\nabla}\times\boldsymbol{n})]^2+K_{33}[\boldsymbol{n}\cdot(\boldsymbol{\nabla}\times\boldsymbol{n})]^2 - \epsilon_0\epsilon_a(\boldsymbol{n}\cdot\boldsymbol{E})^2-\mu_0\chi_a(\boldsymbol{n}\cdot\boldsymbol{H})^2\} \quad \text{(A4)}$$

contains the orientational-elastic Frank energy due to splay (K_{11}), twist (K_{22}), and bend (K_{33}) deformations, and the relevant electric and magnetic parts proportional to the anisotropies of the dielectric permittvity, ϵ_a, and the magnetic susceptibility, χ_a.

Equation (A2) is a generalized Navier-Stokes equation. Its conservative contributions come from the pressure p (which will be eliminated), and from the (negative) Erickson stress

$$\pi_{ij}=\frac{\partial F}{(\partial n_k/\partial x_j)}\frac{\partial n_k}{\partial x_i}. \quad \text{(A5)}$$

The viscous contributions are described by the momentum-flux tensor

$$-T_{ij}^{\rm visc}=\alpha_1 n_i n_j n_k n_l A_{kl}+\alpha_2 n_j N_i+\alpha_3 n_i N_j+\alpha_4 A_{ij}+\alpha_5 n_j n_k A_{ki}+\alpha_6 n_i n_k A_{kj}, \quad \text{(A6)}$$

where $\alpha_1,\ldots,\alpha_6$ are the Leslie coefficients satisfying the Onsager symmetry $\alpha_2+\alpha_3=\alpha_6-\alpha_5$, and $\boldsymbol{N}=(\partial_t+\boldsymbol{v}\cdot\boldsymbol{\nabla})\boldsymbol{n}-\boldsymbol{\omega}\times\boldsymbol{n}$. At last, the electric volume force $\approx\rho\boldsymbol{E}$ is a crucial part in the instability mechanism of the SM.

APPENDIX B: ANALYTIC EXPRESSION FOR THE THRESHOLD OF THE STANDARD MODEL

Here, we use scaled variables and parameters as introduced at the beginning of Sec. III. In the limit of the SM ($\tilde{r}\to\infty$), and using the one-mode approximation (19) and (20), the expression for the neutral surface $R_0^{\rm SM}(q,p)$ can be written as

$$R_0^{\rm SM}=\frac{K^{\rm eff}}{\epsilon_a^{\rm eff}+a_2\sigma_a^{\rm eff}/\eta^{\rm eff}}, \quad \text{(B1)}$$

with the effective orientational elasticity

$$K^{\rm eff}=K_{zz}-\frac{p^2(1-K_{zz})^2 I_2^2}{K_{yy}},$$

$$K_{zz}=K_{33}q^2+K_{22}p^2+1+H_x^2-H_z^2,$$

$$K_{yy}=K_{33}q^2+p^2+4K_{22}+H_x^2-H_y^2, \quad \text{(B2)}$$

the effective anisotropy of the conductivity

$$\sigma_a^{\rm eff}=\frac{\sigma_a}{1+\omega'^2}\left(\frac{\epsilon_q}{\sigma_q}-\frac{\epsilon_a}{\sigma_a}\right), \quad \text{(B3)}$$

$$\omega'=\omega_0\tau_q\epsilon_q/\sigma_q, \quad \text{(B4)}$$

$$\sigma_q=(1+\sigma_a)q^2+p^2+1,\quad \epsilon_q=(1+\epsilon_a)q^2+p^2+1, \quad \text{(B5)}$$

the effective dielectric constant

$$\epsilon_a^{\rm eff}=\epsilon_a(q^2+p^2+1)\left(\frac{\sigma_q^{-1}+\omega'^2\epsilon_q}{1+\omega'^2}\right), \quad \text{(B6)}$$

the effective orientational viscosity coupling the director to the fluid,

$$a_2=-\alpha_2+\alpha_3\left(\frac{1}{q^2}-\frac{\eta_{zy}p^2 I_2}{\eta_{yy}q^3}\right), \quad \text{(B7)}$$

and the effective viscosity

$$\eta^{\rm eff}=\frac{\eta_z^{\rm eff}}{1+p^2(1-K_{22})I_2\eta_{zy}a_2'/qK_{yy}\eta_{yy}a_2}, \quad \text{(B8)}$$

$$a_2'=-\alpha_2+\alpha_3\left(\frac{p^2}{q^2}-\frac{\eta_{yy}}{\eta_{zy}}\frac{I_p}{q}\right), \quad \text{(B9)}$$

$$\eta_z^{\rm eff}=\eta_{zz}-\frac{p^2\eta_{zy}^2}{q^2\eta_{yy}}, \quad \text{(B10)}$$

$$\eta_{zz}=\eta_1+(\eta_1+\eta_2+\alpha_1)\frac{I_1}{q^2}+\frac{\alpha_4}{2}\frac{p^2}{q^2}+\eta_2\frac{\lambda_1^4+I_1p^2}{q^4}, \quad \text{(B11)}$$

$$\eta_{yy}=\eta_1+(\eta_1+\eta_2+\alpha_1)\frac{p^2}{q^2}+\frac{2\alpha_4}{q^2}+\eta_2\frac{p^4+4p^2}{q^4}, \quad \text{(B12)}$$

$$\eta_{zy}=(\eta_1+\eta_2+\alpha_1-\alpha_4/2)\frac{I_p}{q}+\eta_2 I_p\frac{4+p^2}{q^3}. \quad \text{(B13)}$$

The viscosities η_1 and η_2 are given in Eq. (16). The projection integrals are

$$I_1=-\int_{\pi/2}^{\pi/2}dz\,C_1\partial_z^2 C_1=1.2465,$$

$$I_2=\frac{2}{\pi}\int_{\pi/2}^{\pi/2}dz\,\cos z\,\partial_z\sin 2z=0.848,$$

$$I_p = \sqrt{\frac{2}{\pi}} \int_{\pi/2}^{\pi/2} dz \; C_1 \partial_z \sin 2z = 1.1119,$$

$$\lambda_1^4 = \int_{\pi/2}^{\pi/2} dz \;\; C_1 \partial_z^4 C_1 = 5.1388. \tag{B14}$$

APPENDIX C: ANALYTIC EXPRESSION FOR THE PREFACTOR C' OF THE HOPF FREQUENCY

With the definitions of Appendix B, the dimensionless prefactor C' of Eq. (22) reads

$$C'^2 = \frac{K_{zz}}{K^{\rm eff} |\lambda_{0z}| \tau_0^{\rm SM}} \left(C_z^2 + \frac{p^2 (1 - K_{22}) I_2 \lambda_{0z}}{q K_{zz} \lambda_{0y}} C_y^2 \right), \tag{C1}$$

$$C_z^2 = \frac{\sigma_a \epsilon_q^2 |\lambda_{0z}|}{\sigma_q^2 \eta_z^{\rm eff} K_{zz}} \left(1 - \frac{\epsilon_a}{\epsilon_q} \frac{\sigma_q}{\sigma_a} \right) \left(a_2 - \frac{\epsilon_a q^2 \eta_z^{\rm eff}}{\epsilon_q} \right), \tag{C2}$$

$$C_y^2 = \frac{\sigma_a \epsilon_q^2 |\lambda_{0y}|}{\sigma_q^2 \eta_z^{\rm eff} K_{yy}} \left(1 - \frac{\epsilon_a}{\epsilon_q} \frac{\sigma_q}{\sigma_a} \right) \frac{\eta_{zy}}{\eta_{yy}} a_2'. \tag{C3}$$

Here, λ_{0z} and λ_{0y} are given by

$$\lambda_{0z} = - \frac{K_{zz} \eta_z^{\rm eff}}{\eta_z^{\rm eff} - a_2^2},$$

$$\lambda_{0y} = - \frac{K_{yy} \eta_z^{\rm eff}}{\eta_z^{\rm eff} (1 - a_2'^2 / \eta_{yy}) - (p^2/q^2)(\eta_{zy}^2 / \eta_{yy}^2) a_2'^2}. \tag{C4}$$

For normal rolls $K^{\rm eff} = K_{zz}$ and $\tau_0^{\rm SM} = -1/\lambda_{0z}$ so that $C'^2 = C_z^2$ is equivalent to the normal-roll expression for $C' := \sqrt{\sigma_a} C$ in Ref. [18], if one identifies $\eta_z^{\rm eff}$ with $1/L_{nn}$ and takes into consideration a printing error in Eq. (38) of Ref. [18]. There, the factor $1 - (\epsilon_a/\epsilon_q) L_{nn} q^2$ should be replaced by $L_{nn} - (\epsilon_a/\epsilon_q) q^2$. Also, in Ref. [18] some terms proportional to the small viscosity α_3 are neglected.

APPENDIX D: EFFECTIVE NONLINEAR WEM EQUATIONS

We here present the elements of an approach that should give a useful starting point in the regime where a weakly nonlinear description of the SM is valid, i.e., for $\epsilon \ll 1$. This range is usually considerably larger than the weakly nonlinear range of the WEM where the CCGL, considered in the main parts of this paper, is applicable. In the derivation of the CCGL, the modes excited at second order were treated adiabatically. This is justified if the relaxation rate $\tilde{r}$ of the slowest excited mode is much higher than the relaxation rate ϵ/τ_0 of the critical modes. In the Hopf regime, this leads to

$$\epsilon \ll \tau_0 \tilde{r} = 2 \Delta \epsilon. \tag{D1}$$

where the threshold shift $\Delta\epsilon$ is typically of the order of $0.01 \cdots 0.05$.

The second-order and the third-order nonlinearities $\boldsymbol{N}_2$ and $\boldsymbol{N}_3$ of Eq. (26) contain, respectively, several hundred and some thousand terms, so a brute-force generalization appears unfeasible. We suggest that in the range $\epsilon \ll 1$, the nonlinearities of the WEM can be simplified without essentially changing the dynamics and propose the following set of equations:

$$\partial_t \begin{pmatrix} \rho \\ \sigma_\perp \\ n_z \\ n_y \\ g \\ f \end{pmatrix} + \text{linear terms} = - \begin{pmatrix} \sigma_a E_0 (\partial_y n_y n_z + \partial_z n_z^2) \\ \boldsymbol{v} \cdot \boldsymbol{\nabla} \sigma_\perp \\ g_1 n_z^3 + g_2 n_z (\partial_x n_z)(\partial_y n_z) \\ 0 \\ 0 \\ 0 \end{pmatrix}. \tag{D2}$$

The left-hand side corresponds to $(\underline{\underline{B}} \partial_t - \underline{\underline{L}}) \boldsymbol{u}$ in Eq. (26). The most important nonlinearity of the WEM is the advection $\boldsymbol{v} \cdot \nabla \sigma_\perp$ of the slow field $\sigma_\perp$. Its effect is to ''advect away'' inhomogeneities in $\sigma_\perp$ by the velocity field of the rolls. Thus it recovers the SM behavior at larger amplitude. The nonlinearity $\propto \sigma_a E_0$ in the charge equation influences essentially the magnitude of the σ mode excited at second order. The nonlinearities in the equation for n_z, with g_1 and g_2 fitted to give the correct coefficients in the SM limit, describe parametrically the nonlinearities of the SM on a weakly nonlinear level.

As a necessary condition, the set (D2) must reproduce the CCGL coefficients of the full equations. In Figs. 2 and 3, the CCGL coefficients calculated from Eq. (D2) are given by dashed lines. Except in the case of very small recombination rates the agreement is quantitative for all four nonlinear coefficients.

APPENDIX E: SWIFT–HOHENBERG-LIKE EQUATIONS

We here make a connection of the CCGL with the modified SH equation recently proposed by Tu to explain the worm state [25]. The equations are of the form

$$\partial_t \phi(\boldsymbol{x},t) = (\epsilon + i\omega_H)\phi - \sigma_{\mathrm{SH}}[(\partial_x^2+q_c^2)^2 + (\partial_y^2+p_c^2)^2 + b_{\mathrm{SH}}(\partial_x^2+q_c^2)(\partial_y^2+p_c^2)]\phi + iv_g[(\partial_x^2+q_c^2) + a_{\mathrm{SH}}(\partial_y^2+p_c^2)]\phi + g_0|\phi|^2\phi + g_1|\phi|^4\phi. \tag{E1}$$

The relevant coefficients of Eq. (E1) in terms of the coefficients of the CCGL (4) are

$$v_g = \frac{v_{gx}}{2q_c}, \quad a_{\mathrm{SH}} = \frac{v_{gy}q_c}{v_{gx}p_c}, \quad b_{\mathrm{SH}} = -2\frac{\xi_{xy}^2 q_c}{\xi_{xx}^2 p_c}, \quad \mathrm{Re}(\sigma_{\mathrm{SH}}) = \frac{\xi_{xx}^2}{4q_c^2}, \quad \mathrm{Im}(\sigma_{\mathrm{SH}}) = \frac{\xi_{xx}^2 b_{xx}}{4q_c^2} - \frac{v_{gx}}{8q_c^3}, \quad g_0 = g(1+ic). \tag{E2}$$

Equation (E1) has fewer coefficients than Eq. (4). Calculating the CCGL from Eq. (E1) with the coeffficients (E2) gives for the rest of the CCGL coefficients the relations

$$\omega_\epsilon = 0, \quad b_{yy} = b_{xy} = b_{xx}, \quad \xi_{yy} = \frac{p_c^2}{q_c^2}\xi_{xx}, \quad h = 2, \quad c_h = 0, \tag{E3}$$

whereas Tu had to assume that $\mathrm{Re}(g_0) < 0$ to describe the worms, we have $g > 0$ in the Hopf range.

[1] W. Helfrich, J. Chem. Phys. **51**, 4092 (1969).
[2] Orsay Liquid Crystal Group, Phys. Rev. Lett. **26**, 1642 (1970); E. Dubois-Violette, P. G. de Gennes, and O. J. Parodi, J. Phys. (Paris) **32**, 305 (1971).
[3] J. L. Ericksen, Arch. Ration. Mech. Anal. **4**, 231 (1960).
[4] F. M. Leslie, Q. J. Mech. Appl. Math. **19**, 357 (1966).
[5] P. de Gennes and J. Prost, *The Physics of Liquid Crystals* (Clarendon, Oxford, 1993); S. Chandrasekhar, *Liquid Crystals* (Cambridge University Press, Cambridge, 1992).
[6] W. Zimmermann and L. Kramer, Phys. Rev. Lett. **55**, 402 (1985).
[7] E. Bodenschatz, W. Zimmermann, and L. Kramer, J. Phys. (France) **49**, 1875 (1988).
[8] L. Kramer, E. Bodenschatz, W. Pesch, W. Thom, and W. Zimmermann, Liq. Cryst. **5**, 699 (1989).
[9] L. M. Blinov, *Electrooptical and Magnetooptical Properties of Liquid Crystals* (John Wiley, New York, 1983).
[10] L. Kramer and W. Pesch, Annu. Rev. Fluid Mech. **27**, 515 (1995); *Pattern Formation in Liquid Crystals*, edited by L. Kramer and A. Buka (Springer, New York, 1996).
[11] S. Kai and K. Hirakawa, Prog. Theor. Phys. Suppl. **64**, 212 (1978).
[12] I. Rehberg, S. Rasenat, and V. Steinberg, Phys. Rev. Lett. **62**, 756 (1989).
[13] I. Rehberg, S. Rasenat, M. de la Torre Juarez, W. Schöpf, F. Hörner, G. Ahlers, and H. R. Brand, Phys. Rev. Lett. **67**, 596 (1991).
[14] M. Dennin, M. Treiber, L. Kramer, G. Ahlers, and D. Cannell, Phys. Rev. Lett. **76**, 319 (1996).
[15] M. Dennin, D. S. Cannell, and G. Ahlers, Mol. Cryst. Liq. Cryst. Sci. Technol., Sect. A **261**, 377 (1995).
[16] I. Rehberg, B. L. Winkler, M. de la Torre Juarez, S. Rasenat, and W. Schöpf, Adv. Solid State Phys. **29**, 35 (1989).
[17] A. Joets and R. Ribotta, Phys. Rev. Lett. **60**, 2164 (1988).
[18] M. Treiber and L. Kramer, Mol. Cryst. Liq. Cryst. Sci. Technol., Sect. A **261**, 311 (1995).
[19] M. Treiber, N. Eber, Á. Buka, and L. Kramer, J. Phys. II **7**, 649 (1997).
[20] M. Treiber, doctoral dissertation (in English), University of Bayreuth (1996).
[21] M. de la Torre Juarez and I. Rehberg, Phys. Rev. A **42**, 2096 (1990).
[22] M. Dennin, G. Ahlers, and D. S. Cannell, Phys. Rev. Lett. **77**, 2475 (1996).
[23] M. Dennin, G. Ahlers, and D. S. Cannell, Science **272**, 388 (1997).
[24] M. Dennin, D. S. Cannell, and G. Ahlers, Phys. Rev. E **57**, 638 (1998).
[25] Y. Tu, Phys. Rev. E **56**, R3765 (1997).
[26] S. Rasenat, G. Hartung, B. Winkler, and I. Rehberg, Exp. Fluids **7**, 412 (1989).
[27] M. C. Cross and P. C. Hohenberg, Rev. Mod. Phys. **65**, 851 (1993).
[28] F. H. Busse and E. W. Bolton, J. Fluid Mech. **146**, 115 (1984).
[29] S. Chandrasekhar, *Hydrodynamic and Hydromagnetic Stability* (Clarendon, Oxford, 1961).
[30] The following we list quantities for I52 at 60 °C and for external frequencies $\omega\tau_q \ll 1$. In the limit of the SM, the threshold is given by $\overline{V}_c^{\mathrm{SM}} = 10.68$ V, $q_c^{\mathrm{SM}} d/\pi = 0.966$, $p_c^{\mathrm{SM}} d/\pi = 0.782$. In the same limit, the coefficients of the CCGL are $\tau_0^{\mathrm{SM}} = 0.217$, $\xi_{xx}^2 = 1.050$, $\xi_{yy}^2 = 0.333$, $\xi_{xy}^2 = 0.117$, $g^{\mathrm{SM}} = 0.50$, $h^{\mathrm{SM}} = 0.98$. For $\tilde{r} \to 0$, the Hopf frequency and the group velocities are $\tilde{\omega}\tau_d = 0.091$, $v_{gx}\tau_d \pi/d = 0.066$, and $v_{gy}\tau_d \pi/d = 0.034$.
[31] P. Manneville, *Dissipative Structures and Weak Turbulence* (Academic Press, New York, 1990).
[32] P. Coullet, S. Fauve, and E. Tirapegui, J. Phys. (France) Lett. **46**, 747 (1985).
[33] H. Sakaguchi, Prog. Theor. Phys. **93**, 491 (1995).
[34] M. Dennin, Ph.D. dissertation, University of Santa Barbara (1995).
[35] F. Hörner, doctoral dissertation, University of Bayreuth, 1997 (unpublished).
[36] H. Riecke, Phys. Rev. Lett. **68**, 301 (1992).
[37] H. Riecke, Physica D **61**, 253 (1992).
[38] G. Briére, R. Herino, and F. Mondon, Mol. Cryst. Liq. Cryst. **19**, 157 (1972).